Desalination and Water Treatment
www.deswater.com
50 (2012) 376–386
December
1944-3994/1944-3986 © 2012 Desalination Publications. All rights reserved
doi: 10.1080/19443994.2012.720411
Taylor & Francis
Taylor & Francis Group

CTAB mediated Mg-doped nano Fe_2O_3: synthesis, characterization, and fluoride adsorption behavior

M. Mohapatra*, T. Padhi, S. Anand, B.K. Mishra

Institute of Minerals and Materials Technology, Bhubaneswar, Orissa 751 013, India
Email: mamata@immt.res.in

Received 8 September 2011; Accepted 18 April 2012

ABSTRACT

Magnesium-doped nano ranged hematite was prepared following surfactant (cationic surfactant cetyltrimethyl ammonium bromide, [CTAB]) mediation–precipitation technique. The chemical composition of the synthesized sample was: Fe 63.8% and Mg 1.35%. Presence of crystalline hematite phase was confirmed from the X-ray diffraction pattern. The transmission electron microscopy (TEM) image showed spherical particles varying in the range of 40–200 nm. Fluoride adsorption studies were carried out in batch mode under different experimental conditions, which included time, pH, and amount of adsorbent and adsorbate. The contact time data were fitted to a number of rate equations. The fluoride adsorption reached a maximum at a pH of 7.0 and then, decreased with further increase of pH. The equilibrium data followed both the Langmuir and Freundlich models. ΔG° values were estimated to be −6.695, −5.399, −3.819, −3.568, and −2.740 kJ/mole at 293, 303, 308, 313, and 323 K, respectively. ΔH° and ΔS° were −47.12 kJ/mole and −138.58 J/mole/deg, respectively. The negative ΔH° value confirmed the adsorption process to be exothermic in nature, while the negative ΔS° indicated decreased randomness at the solid solution interface during adsorption. The fluoride loaded sample was characterized using TEM, selected area electron diffraction, and energy dispersive analysis of x. The present results show that the nano structured Mg-doped hematite synthesized by the present procedure can be regarded as a potential adsorbent for fluoride removal from aqueous solutions, as it can be effectively used at pH values of 5.75 and 7.0 which are applicable to the treatment of actual fluoride contaminated water. Fluoride containing water sample collected from nearby location was tested for defluoridation to establish real time use of adsorbent.

Keywords: Nano hematite; Fluoride; Adsorption; Mg-doping; Kinetics; Isotherms

1. Introduction

Fluoride contamination in ground as well as surface water has become a matter of great concern due to its effects on human health and ecological systems spreading in almost all parts of the world. India is one among them where many states are affected by fluoride pollution [1,2]. The increase in industrial activities contribute toward high fluoride levels in water bodies. Fluoride concentrations between 0.5 and 1 mg/L are considered beneficial for teeth and bones. Serious bones and teeth related problems leading to dental fluorosis which progresses to skeletal/crippling fluorosis would occur on continuous consumption of high fluoride (>1 mg/L) containing water [3]. A number of reviews have recently appeared highlighting the available technologies and advances in research for purification of fluoride containing water [4–8]. Removal of fluoride by adsorption is one of the most

*Corresponding author.

studied processes because of the availability of numerous adsorbents and simple procedures.

Iron oxides/hydroxides form an important group of adsorbents for fluoride mitigation from aqueous solutions [9–13]. In the present times, nano materials are making inroads in almost all fields of technological development. Water purification technologies based on nano materials are gaining tremendous importance [14–17]. Some studies have been reported on synthesis of pure and doped nano iron oxides/hydroxides-based materials and their adsorption behavior for fluoride [18–21]. Recently, several studies have been reported on the synthesis of hematite particles following different routes, which include micro emulsion [22], surfactant assisted hydrothermal [23], solvothermal [24], and precipitation methods using different combinations of reagents [25]. Nano hematite particles have been synthesized for investigating their applications in different fields, such as gas sensing [26], photo-electrochemical generation of hydrogen [27], solar-driven hydrogen generation [28], catalysts [29,30], and magnetic properties [31–33]. Further, it has been reported that by doping the hematite particles with cations, their performance in NO_2 sensing application [34], photo-electrochemical behavior [35], and catalytic activity [36] can be improved. The recent literature on nano scaled hematite particles has shown that (i) the use of surfactant by mediation or through microemulsion results in uniform particle size and (ii) doping of hematite with cations can improve the performance in various applications. Application of synthesized pure/doped hematite nano particles in water purification for fluoride removal from aqueous solutions has not been reported. In the present work, cetyltrimethyl ammonium bromide (CTAB), a cationic surfactant, was used as it has a comparatively smaller molecular structure as a template and Mg(II) ions were coprecipitated with Fe(III) to synthesize α-Fe_2O_3 nano particles. Magnesium was chosen as it is nontoxic, cheap, and easily available. To the best of our knowledge such an adsorbent for fluoride removal has not been reported earlier.

2. Experimental

2.1. Materials

The chemicals used for the synthesis of Mg-doped ferrihydrite nano powder were: $Fe(NO_3)_3{\cdot}9H_2O$, CTAB, and sodium hydroxide of E-Merck, India and $MgCl_2{\cdot}6H_2O$ of Ranbaxy, India. Sodium fluoride (Ranchem, India) was used for the preparation of the standard fluoride (100 mg/L) stock solution. Sodium 2-(para sulfophenyl azo)-1,8-dihydroxy-3,6-naphthalene disulfonate (SPADNS) and zirconyl oxychloride used for fluoride analysis were of GR (E. Merck) grade.

2.2. Preparation of Mg-doped iron oxide sample

A 100 mL of mixed solution containing 55.5 g/L Fe (III) and 1.2 g/L Mg(II) was taken in a beaker. To this, 5 mL of 10% CTAB solution was added (above the critical micelle concentration) and the solution was stirred for 2 h followed by pH adjustment to 10.0 with slow addition of 1 M NaOH. The precipitate was stirred for 24 h. The contents were filtered through a G4 frit crucible and the precipitate was thoroughly washed with distilled water till the filtrate was free of chloride (tested with silver nitrate solution) and nitrate (qualitative ring test for nitrate). The precipitate was then transferred to a beaker and the volume was made up to 500 mL with distilled water. The contents were aged at 333 K for 12 h in an air oven. After aging, the solid was separated by filtering through a G_4 crucible, washed thoroughly with distilled water, and dried in an air oven at 373 K for 24 h. For convenience, the sample has been coded as Mg-H.

2.3. Analysis and characterization

The sample was acid digested and iron was volumetrically analyzed [37]. The pH_{PZC} (point of zero charge) of the synthetic materials was determined following Balistrieri and Murray method [38]. Surface area of the sample was measured using Micromeritics ASAP-2020. The crystal structure of the product was determined by X-ray diffraction (XRD) (Model X'pert Pro-3040/60) using CoKa radiation with $\lambda = 1.79$ Å. The surface morphology of the as prepared and fluoride loaded sample was observed using electron microscopy (FEI, TECNAI G^2 20, TWIN) operating at 200 kV, equipped with a GATAN CCD camera. Samples for transmission electron microscopy (TEM) were prepared by first diluting a small amount of suspension with ethanol, sonicating, and placing a single drop of the resulting suspension onto a 200 mesh carbon-coated copper grid (from SPI suppliers), which was then allowed to dry in air.

2.4. Adsorption studies

A 100 mg/L fluoride stock solution was prepared by dissolving 0.221 g of NaF in 1 L of double distilled water. The experimental solutions were prepared by appropriate dilutions of the above solution. The

sample (0.05 g) was taken in a 100 mL polyethylene plastic vial and a 50 mL of fluoride solution of known concentration was added. The contents were kept for constant shaking in a temperature controlled water bath shaker over a period of predetermined time and the solids were separated by filtration using 0.45 μm membrane. The solutions were collected for analysis and fluoride concentration in the solutions was determined. Fluoride analysis was carried out by following SPADNS method [39] and the color absorbance was measured on UV–visible spectrophotometer.

3. Results and discussion

3.1. Chemical analysis and physico-chemical characterization of the Mg-H sample

Chemical analysis of the sample showed it to contain 63.8% iron and 1.35% magnesium. The point of zero charge pH_{PZC} of the Mg-H sample was determined as 9.25 from the plot of pH_i–pH_f vs. pH (Fig. 1), where pH_i refers to the initial pH of the solution equilibrated for 2 h and pH_f refers to the pH values obtained on addition of known amounts of adsorbent equilibrating for 72 h at room temperature with intermittent shaking [38]. Liu et al. [40] have reported the pH_{PZC} of ferrihydrite to be ~9.2, while Cornell and Schwertmann [41] have reported pH_{PZC} values of 9.2 and 8.5 for hematite and goethite, respectively. Surface area of the sample was estimated as 189 m^2/g.

3.2. XRD studies

The XRD pattern (Fig. 2) of the sample showed very sharp major peaks situated at 2θ values of 27.39, 37.98, 40.89, 47.11, 50.31, 57.26, 62.98, and 67.29 with corresponding d-spacing of 3.77, 2.75 2.56, 2.24, 2.10, 1.86, 1.71, and 1.61 Å corresponding to hematite (JCPDS Card No 33-0664) phase. However, a small peak at 2.14 Å is observed which does not correspond to hematite.

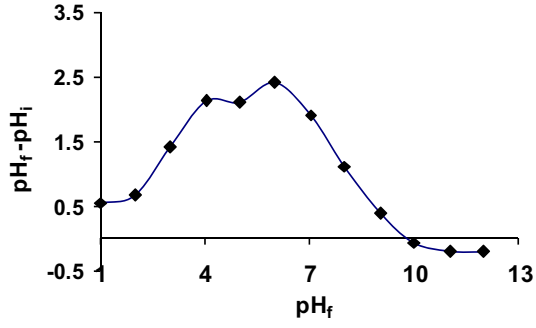

Fig. 1. Plot for pH_f–pH_i vs. pH_f for determining pH_{PZC} of Mg-H sample.

3.3. TEM studies

A typical TEM image is given in Fig. 3. The TEM image shows spherical shaped particles with size varying from 40 to 200 nm.

A comparison of chemical analysis and phase formation of various samples obtained by precipitation of iron oxides/hydroxides using similar conditions (i) in the absence of CTAB and magnesium [42], (ii) in the presence of CTAB [21], and (iii) in the presence of

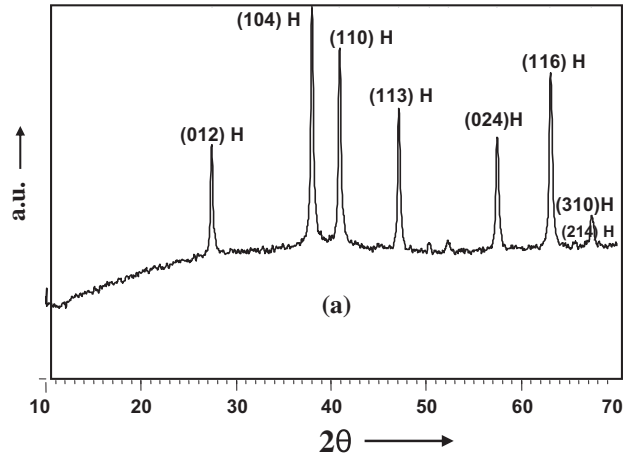

Fig. 2. XRD pattern of Mg-F sample.

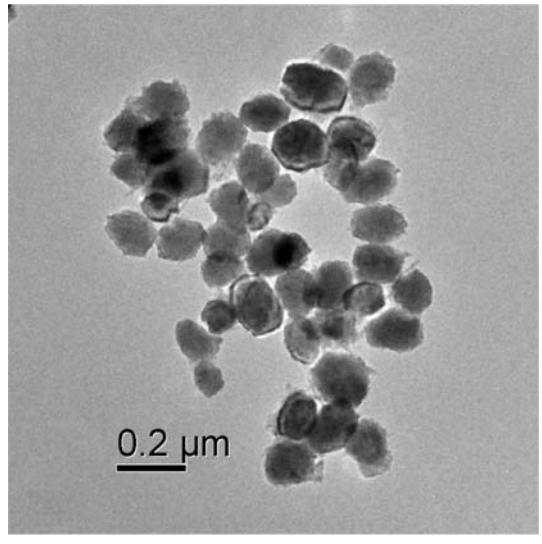

Fig. 3. TEM image of nano sized hematite particles of Mg-H sample.

Table 1
Phase formation under different conditions and point of zero charge pH_{PZC}

pptn. conditions	Chemical analysis		Crystalline phases	pH_{PZC}
	% Fe	% Mg		
No CTAB, No Mg	55.83	_	6-line ferrihydrite	8.0 [42]
CTAB, No Mg	60.13	_	Mixed ferrihydrite, α FeOOH, α-Fe_2O_3	6.95 [21]
CTAB and Mg	63.8	1.35	α-Fe_2O_3	9.25 present work

both CTAB as well as magnesium are given in Table 1. In the absence of surfactant and magnesium, 6-line ferrihydrite was obtained which had shown a very poor response for fluoride uptake hence detailed work was not carried out. When precipitation was carried out by CTAB mediation in the absence of Mg(II) ions, mixed phases of iron oxides containing ferrihydrite, goethite, and hematite were obtained. Detailed studies on fluoride adsorption on the mixed oxides so obtained have been published [21] and will be compared in later section. It is only on surfactant mediation doping of Mg(II) ion hematite phase was formed. The incorporation of Mg(II) ions had either converted goethite to hematite or restricted the formation of goethite for direct conversion of 6-line ferrihydrite to hematite during coprecipitation. Presence of secondary metal ions on the precipitation of iron oxide phases may be governed by a variety of mechanisms that depend on the pH of the system and the ion itself [43]. These include specific and nonspecific adsorption, surface-enhanced precipitation, and bulk precipitation mechanisms. Limited inclusion of Mg(II) together with Fe(III) in a coprecipitated phase is expected considering the similarities in their ionic radii. Indeed, Mg(II) has been observed to be accommodated deeply into the structure of other oxides [44]. Such structural changes would have an impact on surface properties. The increase in Fe% in the samples prepared in the presence/absence of CTAB and/or Mg given in Table 1 is due to the formation of different phases of Fe(III). The sample prepared in the absence of CTAB and Mg has 6-line ferrihydrite as the only phase. The chemical formula for ferrihydrite, $Fe_5HO_8{\cdot}4H_2O$, should have 58.1% Fe, but generally ferrihydrite has intercalated water which reduces the Fe content of the product. While in case of CTAB with no Mg, a mixture of various phases i.e. ferrihydrite (Fe 58.1%), goethite (Fe 62.8%), and hematite (Fe 69.9%) are formed resulting in Fe content of 60.8%. In the presence of CTAB and Mg, primarily hematite phase was formed thereby increasing the Fe content of the prepared sample.

3.4. Fluoride adsorption studies on Mg-H sample

3.4.1. Effect of contact time

Fig. 4(a) shows the fluoride adsorption contact time data at pH 5.75, plotted as % adsorption as a function of time under the conditions: temperature 308 K, fluoride concentration 10 mg/L, and adsorbent concentration 1 g/L. The % F^- adsorption increased from 9.1 to 80.3% as the time increased from 15 to 240 min. Quasi equilibrium state was achieved in 240 min, as over a period of next 240 min only 1% increase in F^- adsorption was observed. The initial rapid adsorption was presumably due to ion exchange (up to 120 min) with surface hydroxyl ions of the adsorbent. The slow adsorption in the later stage represents a gradual uptake of fluoride at the inner surface [45]. The fluoride uptake stabilized after a period of 4 h (240 min). Hence, further study was carried out using 4 h as contact time. The kinetic data were fitted to various models to determine the best fit.

Pseudo-first-order, pseudo-second-order, and Elovich equations were used to determine the kinetic parameters and these are given by Eqs. (1)–(3), respectively.

$$\ln(q_e - q_t) = \ln q_e - k_1 t \quad (1)$$

$$t/q_t = 1/(k_2 q_e^2) + (1/q_e)t \quad (2)$$

$$q_t = \beta \ln(\alpha\beta) + \beta \ln t \quad (3)$$

where q_e and q_t are the amounts of metal ion adsorbed per unit weight of adsorbent at equilibrium and at any time t, respectively (mg/g), k_1 is the rate constant of pseudo-first-order adsorption (1/min), k_2 is the rate constant of pseudo-second-order adsorption (g/mg/min), α is the initial adsorption rate of Elovich equation (mg/g/min), and the parameter β is related to the extent of surface coverage (mg/g) and activation energy for chemisorption [46]. The constants can be

obtained from the slope and intercept of a straight line of qt vs. ln t. The kinetic plot of ln $(q_e - q_t)$ vs. t, t/qt vs. t, and q_t vs. ln t is shown in Fig. 4(b–d), respectively. The kinetic parameters and values of regression coefficients are given in Table 2.

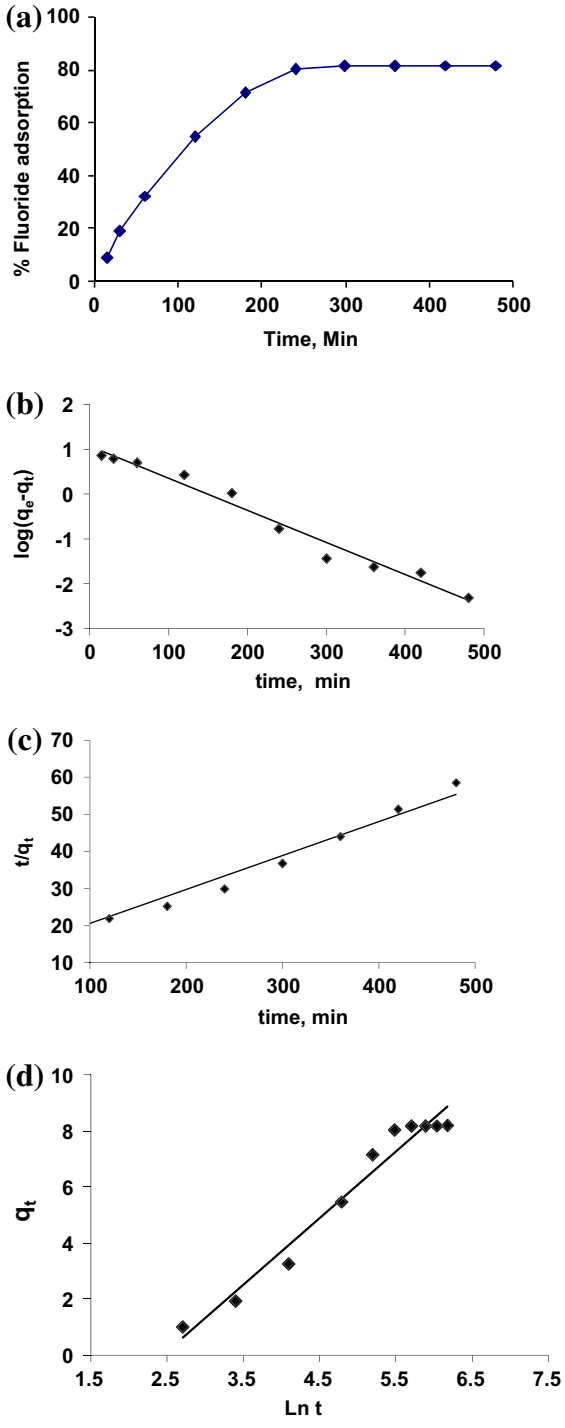

Fig. 4. (a) Effect of contact time on fluoride removal. Conditions: adsorbent dose 1 g/L, initial fluoride concentration 10 mg/L, temperature 308 K, and pH 5.75, (b) pseudo-first-order plot, (c) pseudo-second-order plot and, and (d) Elovich model plots (data correspond to (a).

As observed from the parameters of various models, the regression coefficients values (r^2) of all the models are close to 1. Considering the q_e values, pseudo-second-order model shows less deviations when compared to the value obtained from pseudo-first-order model, it is proposed that the kinetics is better governed by pseudo-second-order model. Such observations have been reported earlier also [47]. The Elovich plot clearly indicates that the model does not fit the contact time data at high ln t values.

To further probe into the possible contribution of intra particle diffusion onto fluoride adsorption, the linear form of intra particle diffusion model given below was used [48]:

$$q_t = k_i t^{1/2} + I \tag{4}$$

where k_i is the intraparticle diffusion rate constant and can be obtained from the slope of the plot of q_t vs. $t^{1/2}$.

The plot given in Fig. 5 gives a straight line with r^2 value of 0.90 with k_i value as 4.276×10^{-1} mg/g/min$^{1/2}$. The initial curve portions are attributed to boundary layer diffusion effect, while the final linear portions are due to intraparticle diffusion effect [49]. It indicates that mechanism of fluoride removal on adsorbents is complex and both the surface adsorption as well as intra-particle diffusion contributes to the rate-determining step [50].

Table 2
Kinetic parameters as determined from various kinetic equations

Experimental q_e (mg/g)	8.2
Kinetic model	
Pseudo-first-order model	
k_1 (1/min)	7.2×10^{-3}
$q_{e,}$ (mg/g)	11.85
r^2	0.976
Pseudo-second-order (linear) model	
k_2 (g/mg/min)	7.28×10^{-4}
q_e (mg/g)	10.92
r^2	0.976
Elovich model	
α (mg/g min)	4.83
β (g/mg)	2.37
r^2	0.966

3.4.2. Effect of pH

The effect of pH on fluoride removal was studied in the range of 2.0–12.0 and the results are shown in Fig. 6. Other conditions maintained were: time 4 h, temperature 308 K, fluoride concentration 10 mg/L, and adsorbent concentration 1 g/L. As the initial solution pH (pH_i) increased from 2.0 to 7.0, the percentage of fluoride adsorption increased from 25.56 to 91.55%.

A decrease in fluoride adsorption from 91.55 to 24.73% was observed with the increase in initial pH from 7.0 to 12.0. The surface charge of the adsorbent surface plays an important role during removal of cations and anions. In the present study, the pH_{pzc} of the adsorbent was estimated to be 9.25. The adsorbent surface will be positively charged at a $pH < pH_{pzc}$ and will be negatively charged at pH values $> pH_{pzc}$. Two factors will influence the adsorption process: (i) formation of HF due to the presence of H^+ ions at low pH resulting in lowering of adsorption and (ii) strongly positive surface at $pH < pH_{pzc}$ should adsorb fluoride with strong electrostatic forces. At low pH values, i.e. 2–4, the first factor can dominate and later the second one, thereby giving an increase in adsorption of fluoride with the increase in pH up to a value of 7.0. IR analysis by Hiemstra and Riemsdijk [51], who investigated adsorption of F^- on goethite, confirmed that the main reactant of such an adsorption process is singly coordinated FeOH groups. At pH > 9.2, the zeta potentials will be negative resulting in repelling the fluoride ions via columbic repulsion. Further, at high pH values (> 7.0) OH^- ions would compete with F^- ions for adsorption. Sujana et al. have reported similar trends for the effect of pH on fluoride adsorption on iron containing geomaterials and mixed Fe-Al mixed amorphous hydroxides [45,52].

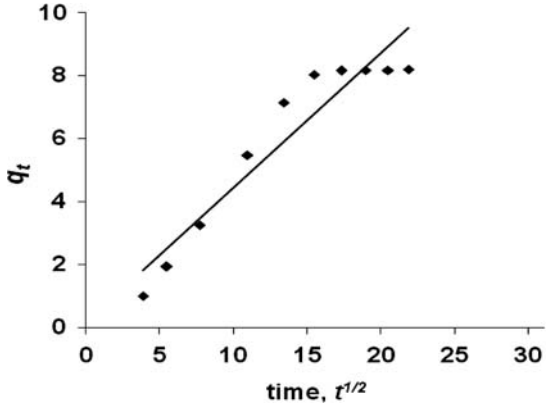

Fig. 5. Plot for q_t vs. $t^{1/2}$ for intra particle diffusion kinetic model.

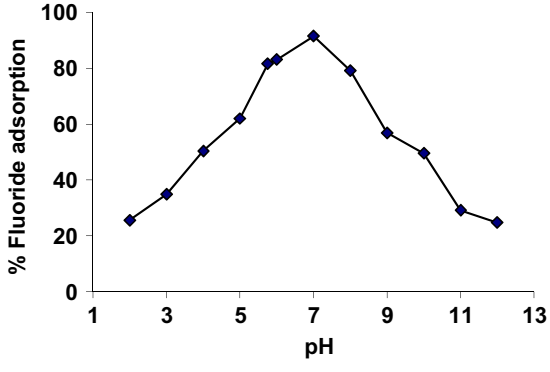

Fig. 6. Effect of solution pH on fluoride removal. Conditions: adsorbent dose 1 g/L, initial fluoride concentration 10 mg/L, temperature 308 K, and contact time 4 h.

3.4.3. Effect of adsorbent dose

The effect of adsorbent dosage on fluoride removal at fixed pH and initial fluoride concentration (10 mg/L) is shown in Fig. 7. It is evident that the percent fluoride removal increased from 43.99 to 97.50% with the increase of the adsorbent concentration from 0.5 to 2.5 g/L, which is due to the fact that a greater amount of adsorbent provides greater number of available binding sites. The decrease in loading capacity is expected as for the same initial concentration of F^- amount of adsorbent increased.

3.4.4. Effect of initial fluoride concentration and isotherm analysis

The fluoride concentration was varied under two different initial pH values: (i) from 10 to 100 mg/L, while the pH, time, and adsorbent concentration were

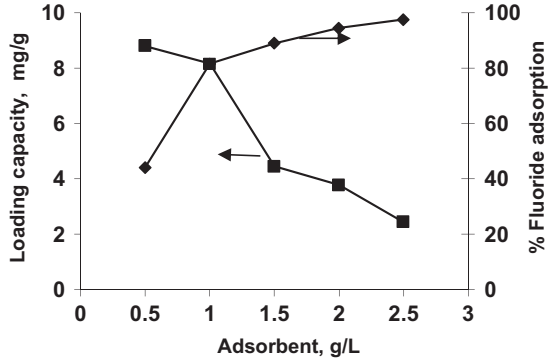

Fig. 7. Effect of adsorbent dose of fluoride removal. Conditions: initial fluoride concentration 10 mg/L, temperature 308 K, pH 5.75, and contact time 4 h.

kept at 5.75, 4 h, and 1 g/L, respectively, and (ii) from 10 to 150 mg/L, while the pH, time, and adsorbent dose were kept at 7.0, 4 h, and 1 g/L, respectively.

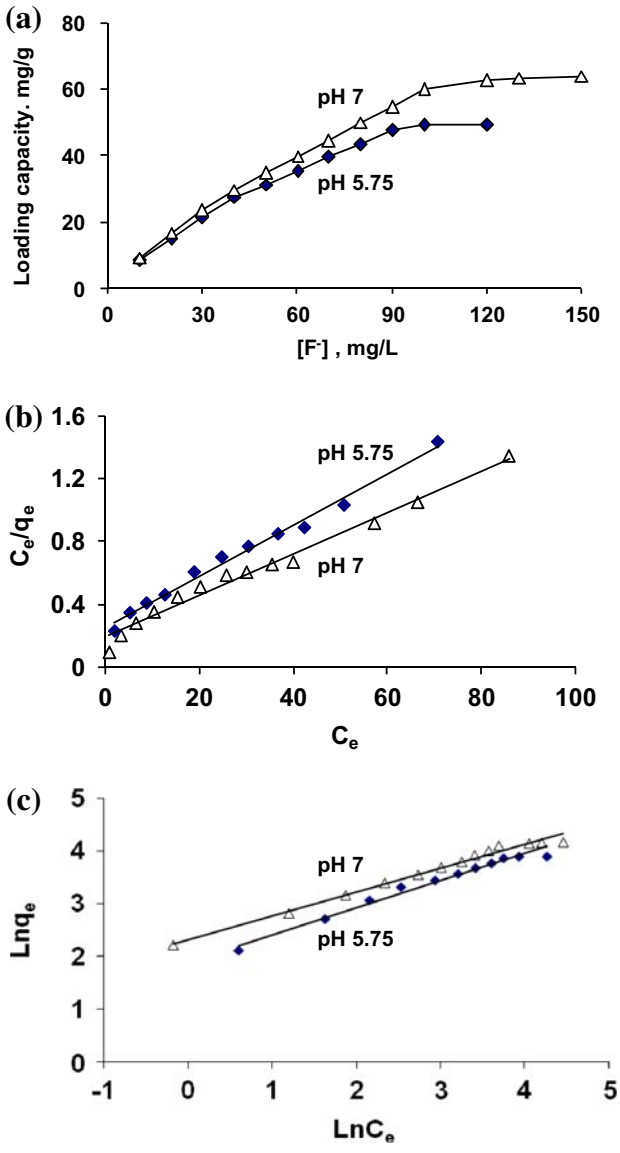

Fig. 8. (a) Effect of initial F^- concentration on its adsorption. Conditions: adsorbent dose 1 g/L, temperature 308 K, pH 5.75, and pH 7.0 contact time 4 h, (b) Langmuir isotherm plots, and (c) Freundlich isotherm plots.

The two pH values were chosen as these are close to the natural pH of water; hence, it was felt necessary to evaluate Langmuir monolayer capacities at both the pH values. The adsorption results are shown in Fig. 8 (a). The maximum loading capacity of 49.2 mg/g was observed till initial F^- concentration of 100 mg/L at a pH of 5.75 and only marginal increase in fluoride uptake was observed with further increase in initial F^- concentration to 120 mg/L. However, at a pH of 7, the loading capacity of 64 mg/g was observed at initial F^- concentration of 150 mg/L.

The isotherm experiments shown in Fig. 8(a) were fitted to the Langmuir and Freundlich models given in Eqs. (5) and (6), respectively.

$$\frac{C_e}{q_e} = \frac{1}{q_m b} + \frac{C_e}{q_m} \tag{5}$$

$$\log q_e = \log K_F + \frac{1}{n}\log C_e \tag{6}$$

where C_e is the equilibrium concentration (mg/L), q_e is the amount adsorbed at equilibrium (mg/g), q_m is the maximum adsorption capacity for Langmuir isotherms, and "b" is an energy term which varies as a function of surface coverage strictly due to variations in the heat of adsorption. $1/n$ and K_F are isotherm constants for Freundlich isotherm. Parameters for Langmuir and Freundlich models were estimated from plots of C_e/q_e vs. C_e and log q_e vs. log C_e shown in Fig. 8(b) and (c), respectively, and are given in Table 3.

At both the pH values, adsorption followed both the models with the correlation coefficients values of ≥ 0.97. The values of the Langmuir equilibrium coefficient, "b", were found to be 0.016 and 0.013 L/g for F^- adsorption at pH of 5.75 and 7, respectively. The Langmuir monolayer capacities were estimated to be 61.3 and 75.2 mg/g at pH of 5.75 and 7, respectively. The Freundlich parameters, K_f, were estimated to be 6.99 and 9.22 at pH 5.75 and 7, respectively, whereas the values of n were 1.94 and 2.22, respectively. In fact, Langmuir isotherm corresponds to a dominant ion-exchange mechanism and reflects monolayer

Table 3
Langmuir and Freundlich parameters for adsorption of fluoride on Mg-H sample

pH	Langmuir coefficients			Freundlich coefficients		
	q_m (mg/g)	b (L/g)	r^2	K_f	n	r^2
5.75	61.3	0.016	0.988	6.99	1.94	0.978
7.0	75.2	0.013	0.982	9.22	2.22	0.986

adsorption, while the Freundlich isotherm shows adsorption–complexation reactions taking place during the adsorption process which could be multilayer and the adsorbent surface may be heterogeneous in nature. In case of formation of only a monolayer and the adsorption process being governed by a combination of ion exchange and complexation reactions, both the isotherms may show goodness of fit to the experimental data. Such observations on fitting of experimental data to both models have been reported by several authors for the adsorption of cations [53–56] or fluoride onto various adsorbents [57,58].

It may be mentioned here that no studies have been reported for F^- adsorption on nano hematite. There is only one reference reporting F^- adsorption on hematite obtained by calcination of waste iron [59]. The authors have reported maximum loading capacity of 24 mg/g. Langmuir monolayer capacity of the sample prepared in the absence of both CTAB and Mg was not determined as the sample did not exhibit good potential for F^- uptake, while in case of mixed oxide obtained by CTAB mediation in the absence of Mg(II) Langmuir monolayer capacity was 53.19 mg/g at a pH of 5.75 [21]. The present adsorbent gave higher Langmuir monolayer capacity.

3.4.5. Effect of temperature and thermodynamic feasibility of the process

The effect of temperature on adsorption was studied in the range of 293–323 K. The data shown in Fig. 9(a) reveal that rise in solution temperature has an adverse effect on fluoride adsorption as with the increase in temperature from 293 to 323 K, % F^- adsorption decreased from 93.98 to 73.50%. The thermodynamic feasibility of the process in the present fluoride-iron oxide system was evaluated from the free energy change following Eq. (7) and the values of the enthalpy change (ΔH°) and the entropy change (ΔS°) of the process were obtained using the van't Hoff equation following Eq. (8):

$$\Delta G^\circ = -RT\ln K_c \quad (7)$$

$$\mathrm{Log}K_c = \Delta S^\circ/2.303\mathrm{R} - \Delta H^\circ/2.303\mathrm{R}T \quad (8)$$

where ΔG° is the change in free energy, T is the absolute temperature in Kelvin, R is the universal gas constant, and K_c is the equilibrium constant at temperature T ($K_c = C_a/C_e$, where C_e is the equilibrium concentration in solution in mg/L and C_a is the adsorbed amount of adsorbate at equilibrium in mg/L).

For each temperature from the experimental values of C_a and C_e, ΔG° values were estimated and were found to be −6.695, −5.399, −3.819, −3.568, and −2.740 kJ/mole at 293, 303, 308, 313 and 323 K, respectively. The van't Hoff plot is shown in Fig. 9(b). From the slope, intercept values of ΔH° and ΔS° were estimated to be −47.12 kJ/mole and −138.58 J/mole/deg. The negative ΔH° value confirms the adsorption process to be exothermic in nature, while the negative ΔS° is indicative of decreased randomness at the solid solution interface during adsorption [60]. In case of F^- adsorption, positive values of ΔS° have been reported in many studies [21,45,52,60].

3.5. Treatment of fluoride containing sample collected from tube well of Nayagarh district of Orissa

The feasibility of using the synthesized sample in real time applications for defluoridation of water was established by purifying a sample containing 5.39 mg/L of fluoride (pH 7.14) collected from a tube well of Nayagarh district of Orissa. The water sample was used as such for the removal of fluoride. Adsorption was carried out under the following conditions: 1 g/L adsorbent dose, temp., ambient, and time 4 h. The

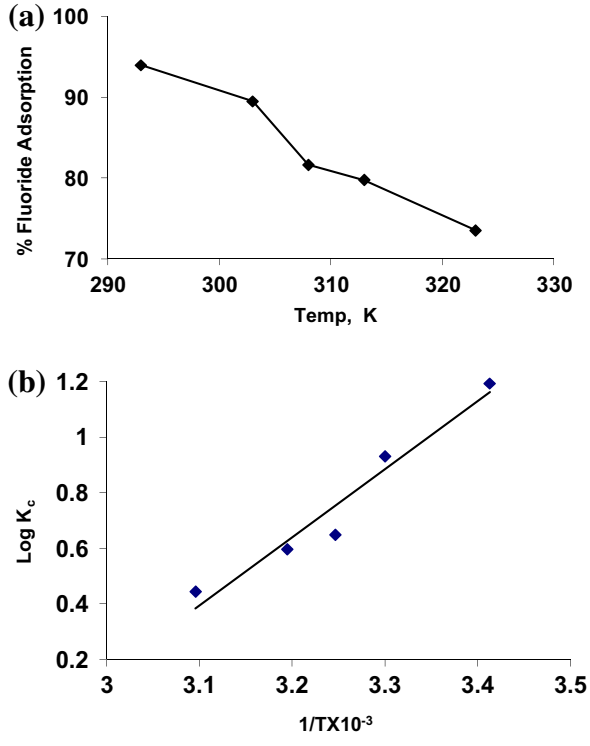

Fig. 9. (a) Effect of temperature on fluoride removal. Conditions: initial fluoride concentration 10 mg/L, adsorbent dose 1 g/L, pH 5.75, and contact time 4 h and (b) van't Hoff plot.

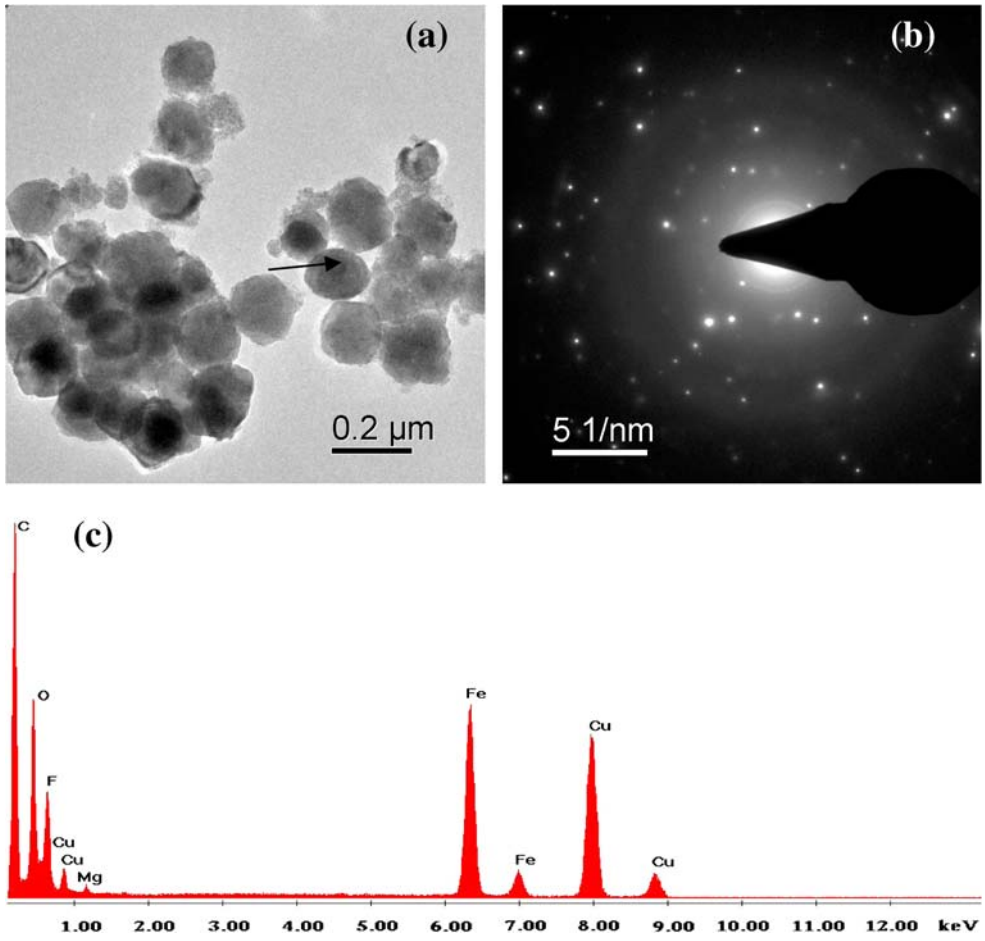

Fig. 10. TEM studies on fluoride loaded samples (a) spherical hematite particle (b) SAED pattern of the arrowed spherical particle (mark hematite planes in SAED), and (c) EDAX pattern.

residual concentration of fluoride was 0.12 mg/L. Further, work needs to be taken up on the following aspects to use the laboratory data for the development of technology: (i) column studies, (ii) regeneration and reuse of the adsorbent, (iii) toxicity characterization leaching procedure test for final disposal after exhaustion of adsorbent, (iv) testing of real fluoride contaminated samples from various locations, (v) cost comparison after generating the data on bench scale which will gives real insight into the operational problems and maintenance costs, and (vi) release of any residual surfactant. The continuous column experiments will give an insight into the probable difficulties due to fine particle nature of the synthesized powder.

3.6. TEM studies on fluoride loaded hematite sample

The morphology of fluoride loaded sample was observed by TEM. It is seen that the particles shape has not changed much as shown in Fig. 10(a). The selected area electron diffraction (SAED) pattern of the arrow head sphere given in Fig. 10(b) shows the planes matching to hematite phase. The energy dispersive analysis of x (EDAX) pattern of spherical particle given in Fig. 10(c) shows the presence of fluorine, magnesium, and iron. The origin of Cu peaks in EDAX pattern is due to the copper grid.

Further, since the synthesized material is hematite which is the most stable form of iron oxides and does not go through any decomposition/phase transformation, it may find application in paint industry as a primer after its exhaustion as an adsorbent. This aspect will also be investigated.

4. Conclusions

Mg-doped nano ranged hematite was prepared following surfactant CTAB mediation–precipitation technique. The XRD pattern showed sharp peaks

corresponding to hematite. The TEM image showed the particle size varying from 40 to 200 nm and the SAED pattern confirmed hematite phase. The fluoride adsorption studies were carried by varying time, pH, temperature, and amount of adsorbent and adsorbate. Various kinetics models were tested for fitting the kinetic data. The fluoride adsorption reached a maximum at a pH of 7.0 and then, decreased with further increase of pH. The equilibrium data followed both the Langmuir and Freundlich models. The Langmuir monolayer capacities were 61.34 and 75.18 mg/g at pH of 5.75 and 7.0, respectively. From the thermodynamic studies, it could be concluded that the fluoride adsorption on Mg-doped nano hematite particles was thermodynamically favorable at low temperatures and was exothermic in nature. The TEM of fluoride loaded sample showed there was not much difference in the morphology of the hematite particles after fluoride adsorption and presence of fluoride was confirmed from the EDAX pattern. The contaminated water collected from Nayagarh district of Orissa was defluoridated in a single stage batch mode.

Acknowledgments

The authors are thankful to Prof. B.K. Mishra, Director, Institute of Minerals and Materials Technology, for his kind permission to publish this paper. We are thankful to Dr. T. Subbaiah, Head, Hydro–electro Metallurgy Department. The financial support provided by DST, India under AISRF scheme is thankfully acknowledged.

References

[1] D. Chakraborti, B. Das, M.T. Murrill, Examining India's groundwater quality management, Environ. Sci. Technol. 45 (2011) 27–33.
[2] WHO, UNICEF, India Assessment, Water Supply and Sanitation-A sponsored study report. Planning Commission, Govt. of India, New Delhi, 2002. http://planningcommission.nic.in/reports/genrep/wtrsani.pdf.
[3] C.B. Dissanayake, The fluoride problem in the groundwater of Sri Lanka—environmental management and health, Int. J. Environ. Stud. 19 (1991) 195–203.
[4] Meenakshi, R.C. Maheshwari, Fluoride in drinking water and its removal, J. Hazard. Mater. 137 (2006) 456–463.
[5] M. Mohapatra, S. Anand, B.K. Mishra, D.E. Giles, P. Singh, Fluoride removal from aqueous media—a review, J. Environ. Manage. 91(1) (2009) 67–77.
[6] A. Bhatnagar, E. Kumar, M. Silanpaa, Fluoride removal from water by adsorption—a review, Chem. Eng. J. 171 (2011) 811–840.
[7] I. Ali, V.K. Gupta, Advances in water treatment by adsorption technology, Nat. Protoc. 1 (2007) 2661–2667.
[8] S. Ayoob, A.K. Gupta, V.T.A. Bhat, A conceptual overview on sustainable technologies for the defluoridation of drinking water, Crit. Rev. Environ. Sci. Technol. 38 (2008) 401–470.
[9] T. Hiemstra, W.H.V. Riemsdijk, Fluoride adsorption on goethite in relation to different types of surface sites, J. Colloid Interface Sci. 225 (2000) 94–104.
[10] S. Dey, S. Goswami, U.C. Ghosh, Hydrous ferric oxide for contaminated water, Water Air Soil Pollut. 158 (2004) 311–323.
[11] M. Streat, K. Hellgardt, N.L.R. Newton, Hydrous ferric oxide as an adsorbent in water treatment: Part 3: Batch and mini-column adsorption of arsenic, phosphorus, fluorine and cadmium ions, Proc. Safe. Environ. Prot. 86(1) (2008) 21–30.
[12] Y. Tang, X. Guan, J. Wang, N. Gao, M.R. McPhail, C.C. Chusuei, Fluoride adsorption onto granular ferric hydroxide: Effects of ionic strength, pH, surface loading, and major coexisting anions, J. Hazard. Mater. 171 (2009) 774–779.
[13] E. Kumar, A. Bhatnagar, M. Ji, W. Jung, S.-H. Lee, S.-J. Kim, G. Lee, H. Song, J.-Y. Choi, J.-S. Yang, B.-H. Jeon, Defluoridation from aqueous solutions by granular ferric hydroxide (GFH), Water. Res. 43(2) (2009) 490–498.
[14] W.-T. Liu, Nanoparticles and their biological and environmental applications, J. Biosci. Bioeng. 102 (2006) 1–7.
[15] P.G. Tratnyek, R.L. Johnson, Nanotechnologies for environmental cleanup, Nano Today 1 (2006) 44–48.
[16] N. Savage, M. Diallo, Nano material and water purification: Opportunities and challenges, J. Nanopart. Res. 7 (2005) 331–342.
[17] Y.C. Sharma, V. Srivastava, V.K. Singh, S.N. Kaul, C.H. Weng, Nano-adsorbents for the removal of metallic pollutants from water and wastewater, Environ. Technol. 30(6) (2009) 583–609.
[18] X. Zhao, J. Wang, F. Wu, T. Wang, Y. Cai, Y. Shi, G. Jiang, Removal of fluoride from aqueous media by Fe_3O_4@Al$(OH)_3$ magnetic nanoparticles, J. Hazard. Mater. 173(1–3) (2010) 102–109.
[19] M. Bhaumik, T.Y. Leswifi, A. Maity, V.V. Srinivasu, M.S. Onyango, Removal of fluoride from aqueous solution by polypyrrole/Fe_3O_4 magnetic nanocomposite, J. Hazard. Mater 186(1) (2011) 150–159.
[20] M. Mohapatra, K. Rout, S.K. Gupta, P. Singh, S. Anand, B.K. Mishra, Facile synthesis of additive-assisted nano goethite powder and its application for fluoride remediation, J. Nano Part. Res. 12 (2010) 681–686.
[21] M. Mohapatra, K. Rout, P. Singh, S. Anand, S. Layek, H.C. Verma, B.K. Mishra, Fluoride adsorption studies on mixed-phase nano iron oxides prepared by surfactant mediation-precipitation technique, J. Hazard. Mater. 186 (2011) 1751–1757.
[22] A. Bumajdad, S. Ali, A. Mathew, Characterization of iron hydroxide/oxide nanoparticles prepared in microemulsions stabilized with cationic/non-ionic surfactant mixtures, J. Colloid Interface Sci. 355(2) (2011) 282–292.
[23] Y. Xu, S. Yang, G. Zhang, Y. Sun, D. Gao, Y. Sun, Uniform hematite α-Fe_2O_3 nanoparticles: Morphology, size-controlled hydrothermal synthesis and formation mechanism, Mater. Letters 65(12) (2011) 1911–1914.
[24] J. Lu, D. Chen, X. Jiao, Fabrication, characterization, and formation mechanism of hollow spindle-like hematite via a solvothermal process, J. Colloid Interface Sci. 303 (2006) 437–443.
[25] Prita P. Sarangi, Bhanudas Naik, N.N. Ghosh, Low temperature synthesis of single-phase α-Fe_2O_3 nano-powders by using simple but novel chemical methods, Powder Technol. 192(3) (2009) 245–249.
[26] J. Huang, M. Yang, C. Gu, M. Zhai, Y. Sun, J. Liu, Hematite solid and hollow spindles: Selective synthesis and application in gas sensor and photocatalysis, Mater. Res. Bull. 46(8) (2011) 1211–1218.
[27] V.R. Satsangi, S. Kumari, A.P. Singh, R. Shrivastav, S. Dass, Nanostructured hematite for photoelectrochemical generation of hydrogen, Int. J. Hydrogen Energy 33(1) (2008) 312–318.

[28] Sina Saremi-Yarahmadi, Bala Vaidhyanathan, K.G. Upul Wijayantha, Microwave-assisted low temperature fabrication of nanostructured α-Fe_2O_3 electrodes for solar-driven hydrogen generation, Int. J. Hydrogen Energy 35 (2010) 10155-10165.
[29] I.V. Chernyshova, S. Ponnurangam, P. Somasundaran, Effect of nanosize on catalytic properties of ferric (hydr)oxides in water: Mechanistic insights, J. Catal. 282(1) (2011) 25–34.
[30] Zhong-Yong Yuan., Tie-Zhen Ren, Su. Bao-Lian, Surfactant mediated nanoparticle assembly of catalytic mesoporous crystalline iron oxide materials, Catal. Today 93–95 (2004) 743–750.
[31] K.K. Sahu, C. Rath, N.C. Mishra, S. Anand, R.P. Das, Microstructural and magnetic studies on hydrothermally prepared hematite, J. Colloid Interface Sci. 185 (1997) 402–410.
[32] Marin Tadić., Nada Čitaković, Matjaž Panjan, Zoran Stojanović, Dragana Marković, Vojislav Spasojević, Synthesis, morphology, microstructure and magnetic properties of hematite submicron particles, J. Alloys Compd. 509(28) (2011) 7639–7644.
[33] Yu-Lin Min, Hong-Yu Xia, You-Cun Chen, Yuangguang Zhang, Ascorbic acid-assisted synthesis of hematite microstructures and magnetic properties, Colloids Surface. A: Physicochem. Eng. Aspects 368(1–3) (2010) 1–5.
[34] J.-M. Tulliani, C. Baroni, C. Lopez, L. Dessemond, New NOx sensors based on hematite doped with alkaline and alkaline-earth elements, J. Eur. Ceram. Soc. 31(13) (2011) 2357–2364.
[35] Ayoung Bak, Wonyong Choi, Hyunwong Park, Enhancing the photo-electrochemical performance of hematite (α-Fe_2O_3) electrodes by cadmium incorporation, Appl. Catal. B: Environ. 110 (2011) 207–215.
[36] Márcia de Souza Ramos, Manuela de Santana Santos, Lucimar Pacheco Gomes, Alberto Albornoz, Maria do Carmo Rangel, The influence of dopants on the catalytic activity of hematite in the ethylbenzene dehydrogenation, Appl. Catal. A: General 341(1–2) (2008) 12–17.
[37] A.I. Vogel, A Text Book of Quantitative Inorganic Analysis, English Language Book Society, Longmans Green, London, 2000.
[38] L.S. Balistrieri, J.W. Murray, The surface chemistry of goethite α-FeOOH in major ion seawater, J. Am. Chem. Soc. 28 (1981) 788–806.
[39] Water and Wastewater Monitoring Analysis Method, fourth Ed., China. Environmental Science Press, 4 (2002) 193–195.
[40] H. Liu, W. Yu, Y. Sun, The formation of hematite from ferrihydrite using Fe(II) as a catalyst, J. Mol. Catal. A: Chem. 226 (2005) 135–140.
[41] R.M. Cornell, U. Schwertmann, The Iron Oxides: Structure, Properties, Reactions, Occurrence and Uses. VCH Verslagsgesellschaft, Weinheim, 1996.
[42] M. Mohapatra, T. Padhi, T. Dash, P. Singh, S. Anand, B.K. Mishra, Cation sorption on nano structured high surface area 6-line ferrihydrite, Toxicol. Environ. Chem. 93(5) (2011) 844–859.
[43] M.M. Benjamin, Adsorption and surface precipitation of metals on amorphous iron oxyhydroxide, Environ. Sci. Technol. 17 (1983) 686–692.
[44] K. Baltpurvins, R. Burns, G. Lawrance, Effect of Ca^{2+}, Mg^{2+}, and anion type on the aging of Iron(III) hydroxide precipitates, Environ. Sci. Technol. 31 (1997) 1024–1032.
[45] M.G. Sujana, H.K. Pradhan, S. Anand, Studies on sorption potential of some geomaterials for fluoride removal from aqueous solutions, J. Hazard. Mater. 161(I) (2009) 120–125.
[46] H. Teng, C. Hsieh, Activation energy for oxygen chemisorption on carbon at low temperatures, Ind. Eng. Chem. Res. 38 (1999) 292–297.
[47] M.G. Sujana, S. Anand, Fluoride removal from ground waters with hydrous Fe/Al mixed hydroxides—Effect of adsorbent and other anion concentration, Appl. Surf. Sci. 256(23) (2010) 6956–6962.
[48] W.J. Weber, J.C. Morris, Equilibria and capacities for adsorption on carbon, Sanitary Eng. Div. 90 (1964) 79–91.
[49] G. McKay, M.J. Bino, Fixed bed adsorption for the removal of pollutants from water, Environ. Pollut. 66 (1990) 33–53.
[50] M. Mahramanlioglu, I. Kizilcikli, I.O. Bicer, Adsorption of fluoride from aqueous solution by acid trated spent bleaching earth, J. Fluorine Chem. 115 (2002) 41–47.
[51] T. Hiemstra, W.H.V. Riemsdijk, Fluoride adsorption on goethite in relation to different types of surface sites. J. Colloid Interface Sci. 225 (2000) 94–104.
[52] M.G. Sujana, G. Soma, N. Vasumathi, S. Anand, Studies on fluoride adsorption capacities of amorphous Fe/Al mixed hydroxides oxides from aqueous solutions, J. Fluorine Chem. 130(8) (2009) 749–754.
[53] K.S. Rao, S. Anand, P. Venkateswarlu, Kinetic, isothermic and thermodynamic studies for Cd(II) adsorption from aqueous solution on *Ficus Religiosa* leaf powder and characterization of loaded biosorbent, Clean: Soil Air and Water 39(4) (2011) 384–391.
[54] T. Tay, M. Candan, M. Erdem, Y. Çimen, H. Türk, Biosorption of cadmium ions from aqueous solution onto non-living lichen ramalina fraxinea biomass, Clean: Soil, Air, Water 37 (3) (2009) 249–255.
[55] M. Mohapatra, K. Rout, B.K. Mohapatra, S. Anand, Sorption behavior of Pb(II) and Cd(II) on iron ore slime and characterization of metal ion loaded sorbent, J. Hazard. Mater. 166 (2009) 1506–1513.
[56] M. Mohapatra, T. Padhi, T. Dash, P. Singh, S. Anand, B.K. Mishra, Cation sorption on nano structured high surface area 6-line ferrihydrite, Toxicol. Environ. Chem. 93(5) (2011) 844–859.
[57] N. Viswanathan, C.S. Sundaram, S. Meenakshi, Removal of fluoride from aqueous solution using protonated chitosan beads, J. Hazard. Mater. 161 (2009) 423–430.
[58] G.E.J. Poinern, M.K. Ghosh, Y.-J. Ng, T.B. Issa, S. Anand, P. Singh, Defluoridation behavior of nano-structured hydroxyapatite synthesized through an ultrasonic and microwave combined technique, J. Hazard. Mater. 185(1) (2011) 29–37.
[59] Y.-H. Huang, Y.-J. Shih, C.-C. Chang, Adsorption of fluoride by waste iron oxide: The effects of solution pH, major coexisting anions, and adsorbent calcination temperature, J. Hazard. Mater. 186 (2011) 1355–1359.
[60] M. Sarkar, A. Banerjee, P.P. Pramanick, A.R. Sarkar, Use of laterite for removal of fluoride from contaminated drinking water, J. Colloid Interface Sci. 302 (2006) 432–441.